Low-temperature structural and transport anomalies in Cu₂Se

Hang Chi,[1] Hyoungchul Kim,[2,7] John C. Thomas,[3] Guangsha Shi,[3] Kai Sun,[3] Milinda Abeykoon,[4] Emil S. Bozin,[4]
Xiaoya Shi,[4] Qiang Li,[4] Xun Shi,[5] Emmanouil Kioupakis,[3] Anton Van der Ven,[3,6] Massoud Kaviany,[2] and Ctirad Uher[1,*]

[1]*Department of Physics, University of Michigan, Ann Arbor, Michigan 48109, USA*
[2]*Department of Mechanical Engineering, University of Michigan, Ann Arbor, Michigan 48109, USA*
[3]*Department of Materials Science and Engineering, University of Michigan, Ann Arbor, Michigan 48109, USA*
[4]*Condensed Matter Physics and Materials Science Department, Brookhaven National Laboratory, Upton, New York 11973, USA*
[5]*State Key Laboratory of High Performance Ceramics and Superfine Microstructure, Shanghai Institute of Ceramics,*
Chinese Academy of Sciences, 1295 Dingxi Road, Shanghai 200050, China
[6]*Materials Department, University of California, Santa Barbara, California 93106, USA*
[7]*High-Temperature Energy Materials Research Center, Korea Institute of Science and Technology, Seoul 136-791, Republic of Korea*

Through systematic examination of symmetrically nonequivalent configurations, first-principles calculations have identified a new ground state of Cu₂Se, which is constructed by repeating sextuple layers of Se-Cu-Cu-Cu-Se. The layered nature is in accord with electron and x-ray diffraction studies at and below room temperature and also is consistent with transport properties. Magnetoresistance measurements at liquid helium temperatures exhibit cusp-shaped field dependence at low fields and evolve into quasilinear field dependence at intermediate and high fields. These results reveal the existence of weak antilocalization effect, which has been analyzed using a modified Hikami, Larkin, and Nagaoka model, including a quantum interference term and a classical quadratic contribution. Fitting parameters suggest a quantum coherence length L of 175 nm at 1.8 K. With increasing temperature, the classical parabolic behavior becomes more dominant, and L decreases as a power law of $T^{-0.83}$.

Transition metal chalcogenides (TMCs) allow fruitful research in contemporary condensed matter physics, leading to intriguing discoveries and promising applications [1]. For example, the silver chalcogenides (e.g., Ag₂Te) are renowned for their extraordinary large magnetoresistance (MR) [2] and have been recently identified as a new class of binary topological insulators (TI) with a highly anisotropic Dirac cone [3]. Additionally, transition metal dichalcogenides (TMDCs) MX_2, where M is a transition metal element and X is a chalcogen atom (S, Se, or Te), are well known for their two-dimensional (2D) structures formed by X-M-X layers with strong in-plane bonding and weak out-of-plane interactions. The unique intrinsic 2D nature of TMDCs has stimulated the search for novel states of matter, for instance, by offering a coexistence of superconductivity and the Mott commensurate charge density wave (CCDW) phase in 1T-TaS₂ [4]. Furthermore, the electronic band structures of TMDCs are believed to host exotic spin-orbit phenomena such as the systematic crossover from weak antilocalization (WAL) to weak localization (WL) [5,6].

As an important member of the TMC family, the superionic Cu₂Se has also received heightened attention in recent developments of thermoelectrics [7] and optoelectronics [8] due to the unique transport properties associated with its structural phase transition occurring at ∼400 K. The exact temperature of this well-known reversible second-order phase transition from the ordered room temperature (RT) monoclinic α phase to the disordered high temperature (HT) cubic β phase depends on the Cu deficiency in the metal sublattice [9] and is found to be tunable upon iodine doping on the selenium sites [10]. It is generally accepted that the disordered

HT β phase of Cu₂Se [space group $Fm\bar{3}m(O_h^5,\#225)$] is constructed by statistically distributing Cu atoms over the 8c tetrahedral sites in a face-centered cubic (fcc) matrix formed by Se atoms. However, the structural determination of the ordered phase(s) still remains controversial [11]. Furthermore, despite some rare reports on samples with quite high Cu deficiency (e.g., Cu$_{2-x}$Se, $0.20 \leqslant x \leqslant 0.25$) [12], a detailed study of the transport properties of stoichiometric Cu₂Se at low temperatures is still desirable. In this paper, we report first-principles determination of the ground state along with several unexpected experimental findings regarding the low-temperature transport properties of Cu₂Se, which may indicate an intrinsic 2D quantum behavior.

The ground state of Cu₂Se was obtained via structural relaxation of the cubic HT β phase. In order to determine the most stable structure, Cu atoms were randomly distributed onto the 32f trigonal sites in the fcc Se matrix, which form tetrahedrons around the 8c tetrahedral sites. Note that for stoichiometric Cu₂Se, only one-quarter of the 32f sites are occupied by Cu atoms. Symmetrically distinct configurations with up to eight Cu atoms have been studied based on the Cu occupancy on the sublattice [13]. Subsequent density functional theory (DFT) calculations of the formation energy have allowed us to identify stable configurations of Cu₂Se. The DFT-based energies were obtained using the Vienna *Ab initio* Simulation Package (VASP) [14] within the Perdew-Burke-Ernzerhof (PBE) parameterization of the generalized gradient approximation (GGA) for exchange and correlation [15] and using the projector-augmented wave (PAW) method [16,17]. The electronic band structure and density of states (D_e) were calculated using more advanced Heyd-Scuseria-Ernzerhof (HSE06) hybrid functional [18,19]. VASP and PHONON [20] codes were then used for the *ab initio* phonon calculations.

*Corresponding author: cuher@umich.edu

TABLE I. Calculated properties of Cu_2Se. The literature results are also listed. ΔE_0 (eV/u.f.), E_g (eV), $u_{p,g,A}$ (m/s), c_{ij} (GPa), and c_p (J/mol-K, at 300 K) are the formation energy per unit formula with respect to the proposed structure, electronic band gap, averaged acoustic phonon group velocity, elastic constants, and specific heat capacity.

	ΔE_0		E_g	$u_{p,g,A}$	c_p	c_{11}	c_{22}	c_{33}	c_{44}
Cu_2Se	0		1.03	2635	72.1	11.14	102.49	88.62	36.75
Literature	0.003[a]	0.046[b]	1.20[c]	2918[d]	81.6[e]	–	–	–	–
	c_{55}	c_{66}	c_{12}	c_{13}	c_{23}	c_{15}	c_{25}	c_{35}	c_{46}
Cu_2Se	14.65	12.82	6.81	6.90	42.37	−5.10	14.51	22.42	11.30
Literature	–	–	–	–	–	–	–	–	–

[a] $P2_1/c$ structure, from Ref. [23].
[b] $C2/c$ structure, from Ref. [10].
[c] From Ref. [21].
[d] From Ref. [7].
[e] From Ref. [22].

The total energy and Hellmann-Feynman (HF) forces were found starting from the fully relaxed configuration, such that initial ionic forces were less than 10^{-5} eV/Å. The ionic displacements of 0.03 Å of selected atoms were sampled along the x, y, and z directions. All phonon and thermodynamic properties were predicted using a fit of interatomic force constant tensors to the calculated HF forces. Diagonalization of the dynamical matrix yields the phonon dispersion from which the density of states (D_p) was obtained. Physical properties of Cu_2Se are summarized in Table I, with the literature results also listed [21,22].

The proposed ground state of Cu_2Se crystallizes in space group $P2_1/c(C_{2h}^5,\#14)$, with optimized lattice parameters $a = 7.453$ Å, $b = 4.322$ Å, $c = 6.880$ Å, $\alpha = 90.00°$, $\beta = 70.62°$, $\gamma = 90.00°$, and atomic occupation Cu1 (0.06111, 0.58259, 0.15164), Cu2 (0.80599, 0.92292, 0.05310), and Se (0.28070, 0.93855, 0.25485). As shown in Fig. 1(a), the ground state of Cu_2Se has quasi-2D characteristics typified by the Se-Cu-Cu-Cu-Cu-Se type of sextuple layers (thickness $t = 3.95$ Å), which are interconnected via weak Se-Se bonds (gap $\delta = 3.08$ Å). Compared with recent literature results using rather different approaches, the monoclinic structure of Cu_2Se obtained here has lower formation energy per unit formula (Table I) [10,23]. The proposed structure is also dynamically stable due to the absence of the soft modes in the phonon spectrum, as is evident in Fig. 1(d). As shown in Fig. 1(e), the monoclinic Cu_2Se is confirmed to be semiconducting, and the electronic band gap E_g (using HSE) is found to be 1.03 eV, which agrees very well with the experimental value of 1.20 eV [21] and is the best first-principles result in comparison to the existing literature values [24].

Polycrystalline Cu_2Se samples were prepared following the recipes described elsewhere [10]. Powdered samples were used for the temperature-dependent x-ray diffraction (XRD) experiments at the X17A beamline of the National Synchrotron Light Source at the Brookhaven National Laboratory. The setup utilized cylindrical geometry with an x-ray beam of 67.42 keV ($\lambda = 0.1839$ Å), a Perkin-Elmer image plate detector placed perpendicular to the primary beam path $d = 204.134$ mm away from the Kapton capillary containing the pulverized sample, and an Oxford Cryosystem 700 for temperature control. A JEOL 2010F transmission electron microscope (TEM) operating at 200 kV was used to

collect selected area electron diffraction (SAED) patterns for the analysis of the detailed microstructure. Simulated SAED patterns were obtained using the CrystalKit software package.
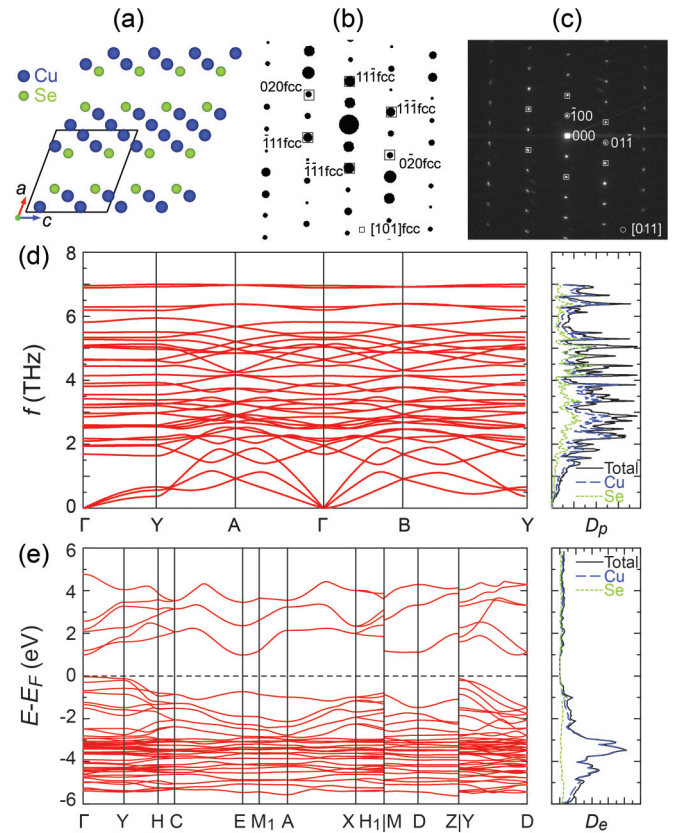

FIG. 1. (Color online) (a) Projected (along the monoclinic b axis) *ab initio* ground state structure of Cu_2Se formed by repeating sextuple layers of Se-Cu-Cu-Cu-Cu-Se. (b) Simulated SAED pattern along the zone axis [011] of the monoclinic phase and the $[101]_{fcc}$ with the diffractions from the fcc structure labeled as squares. (c) The experimental SAED pattern along the [011] zone axis of the monoclinic phase. (d) The calculated phonon band structure and density of states (D_p) indicate the proposed structure is dynamically stable. (e) The electronic band structure and density of states (D_e) calculated using HSE hybrid functional suggests that Cu_2Se is a semiconductor with band gap $E_g = 1.03$ eV.
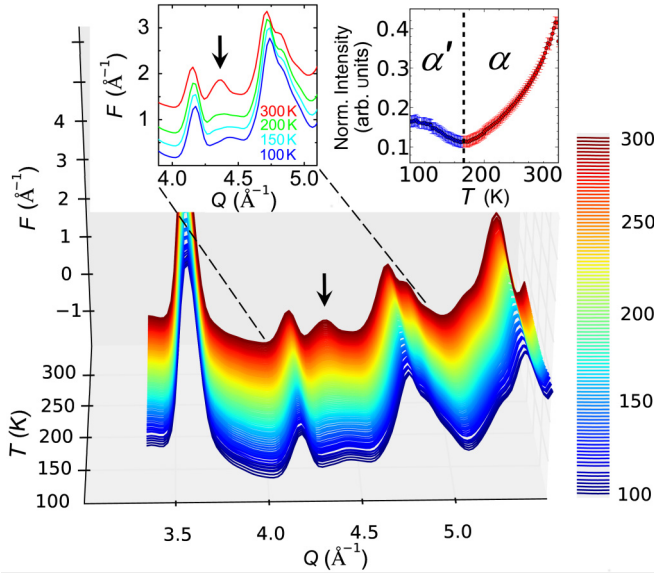
FIG. 2. (Color online) Reduced total scattering XRD structure function, $F(Q) = Q[S(Q) - 1]$, where $S(Q)$ is the total scattering structure function and Q is the momentum transfer, in the 100–300 K range (main panel). Temperature evolution of the normalized intensity around (400) reflection in cubic notation, marked with an arrow in the upper left inset ($Q \sim 4.3$ Å^{-1}). This region is sensitive to subtle structural changes and evidences the α' to α superstructure transition at around 175 K, as denoted by a vertical dashed line (upper right inset). Red symbols denote the evolution with temperature of the intensity peaked at $Q \sim 4.362$ Å^{-1}, while the blue symbols show the evolution of the intensity peaked at $Q \sim 4.436$ Å^{-1}.

FIG. 3. (Color online) Low-temperature transport profile of sto-ichiometric Cu_2Se as a function of temperature. (a) Electrical resistivity ρ and Hall coefficient R_H show anomalies at 100–150 K, where ρ measurements overlap upon either warm-up or cooldown in the temperature. (b) Hall density p and Hall mobility μ_H.

The chemical composition analyses were conducted using energy dispersive spectrometry (EDS). The low-temperature transport property measurements were carried out in the temperature range of 1.8–300 K on samples with dimensions $6 \times 2 \times 1$ mm^3 in a Quantum Design Magnetic Property Measurement System (MPMS) (magnetic field up to 5.5 T) using a Linear Research ac bridge with 16 Hz excitation.

The EDS analysis on the TEM specimen indicates it contains 66.3 at.% Cu and 33.7 at.% Se, which verifies the Cu_2Se chemical composition. The simulated SAED pattern along the monoclinic [011] zone axis is presented in Fig. 1(b), where the monoclinic [011] axis of the proposed ground state is equivalent to an fcc [101] axis. Spots labeled by the square symbols are indexed according to the fcc diffraction pattern, which corresponds to the SAED pattern of the HT cubic β phase [10]. Figure 1(c) displays the experimental SAED pattern along the monoclinic [011] axis. The agreement between the experimental and theoretical patterns has verified the predicted layered structure of the ground state. Additional superstructural diffraction spots/stripes have been also observed along other zone axes. This may result from the different packing order of the sextuple layers and/or Cu-vacancy ordering at finite temperature when thermal energy starts to affect the structure [25].

To further understand the structure, low-temperature XRD measurements have been performed. In line with earlier reports [12,25–28], a reversible α to α' superstructure transition is also evident in the sample studied here via an intensity
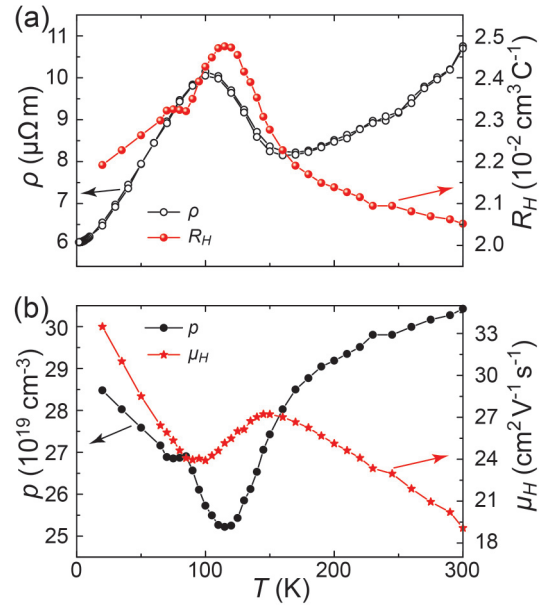
rearrangement of the multiplet of superlattice peaks located in the Q region close to the (400) reflection in cubic notation (Fig. 2). This is found from the assessment of the systematic temperature-dependent XRD data, collected in the 100–300 K range upon warming. The transfer of intensity occurs at around 175 K (upper right inset in Fig. 2).

We were interested to find out what the impact is of such structural changes on the transport properties. As shown in Fig. 3, the above mentioned α to α' type of transition has a strong imprint on the temperature dependence of the electrical resistivity (20% effect) and the Hall effect. The electrical resistivity of Cu_2Se exhibits a highly anomalous behavior in the 100–150 K temperature range, which is also accompanied by a large peak in the Hall effect. We speculate that such features might represent a possible charge density wave (CDW) transition [29] as a result of the distortion/redistribution of the sextuple layers upon temperature change. However, further theoretical and experimental efforts are needed to clarify the issue. We note that in spite of looking for accompanying anomalies in the Seebeck effect, thermal conductivity, and the specific heat, we found none. The anomalous behavior seems to be limited to galvanomagnetic transport only.

At even lower temperatures (1.8–30 K), the MR of Cu_2Se is extraordinary, as shown in Fig. 4(a). The semiclassical transport theory predicts a quadratic field-dependent MR in the low-field range, which saturates in high fields. In distinct contrast to the traditional theory, the MR of Cu_2Se at low temperatures exhibits a WAL-like cusp, which is suppressed when the temperature increases. In addition, at high fields, the MR increases with the increasing field in a linear fashion with no sign of saturation up to $B = 5$ T.

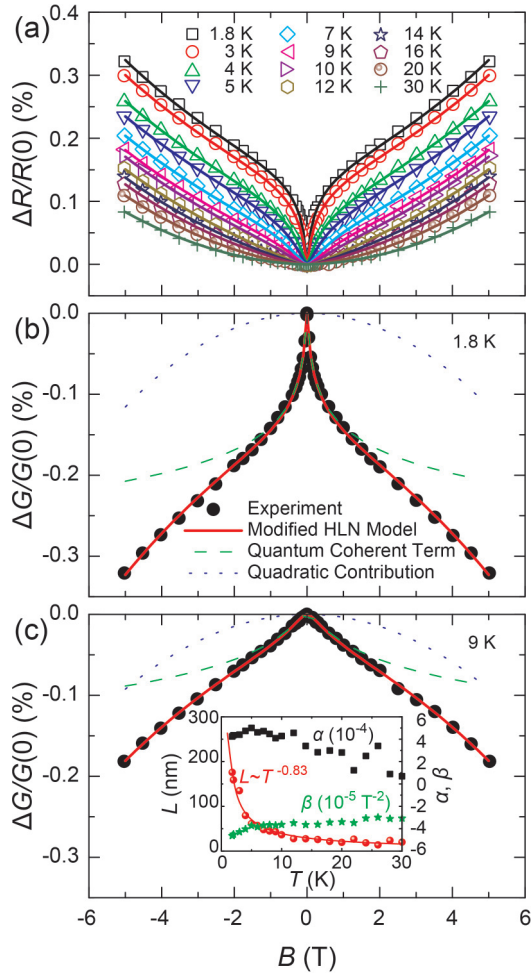We account for the field dependence of differential magnetoconductance (MC) over the entire range of fields and

FIG. 4. (Color online) (a) Magnetoresistance profile (as a function of magnetic field intensity) of Cu_2Se at various temperatures (1.8–30 K) indicating evolution of weak antilocalization behavior as the temperature is lowered to 1.8 K. Theoretical fitting to differential magnetoconductance using a modified HLN model at selected temperatures (b) 1.8 K and (c) 9 K. The inset of (c) depicts the fitting parameters showing a power law behavior ($\sim T^{-0.83}$) of the quantum interference length.

temperatures with a modified Hikami, Larkin, and Nagaoka (HLN) quantum interference model [30,31]:

$$MC \equiv \frac{G(B) - G(0)}{G(0)}$$

$$= -\alpha \left[\psi \left(\frac{\hbar}{4eL^2 B} + \frac{1}{2} \right) - \ln \left(\frac{\hbar}{4eL^2 B} \right) \right] + \beta B^2,$$

$$(1)$$

where ψ is the digamma function. The original formalism of the simple HLN model was developed to characterize the transport properties of a 2D system where the conductance quantum ($2e^2/h$) naturally comes into play. In order to compensate for the bulk effects of this quasi-2D layered structure of Cu_2Se, we have normalized the conductance using the zero field value and introduced a dimensionless fitting parameter α. Here L is the phase coherence length, and β is the quadratic coefficient arising from additional scattering terms. The HLN model has been successfully used in explaining the magnetotransport phenomena in various 2D material systems like Bi_2Se_3 [32,33], Bi_2Se_2Te [34], and Bi_2Te_2Se thin films [31]. It is worth emphasizing that such a modified model simultaneously accounts for the quantum phase interference cusp at low fields as well as the linearlike MR at high fields. It is shown that the additional quadratic term compensates the logarithmic dependence of the quantum interference at high fields, leading to an intermediate linear field dependence of MR. The overall fitting result, along with the corresponding quantum interference term and quadratic term, is shown in Figs. 4(b) and 4(c) for $T = 1.8$ K and 9 K, respectively. In the present sample, the phase coherence length L is 175 nm at 1.8 K and decreases following a power law of $T^{-0.83}$ temperature dependence. The successful application of the HLN model in Cu_2Se is advocating for the 2D quantum nature of the new phase and likely provides another candidate of bulk materials with monolayer behavior, apart from the newly discovered ReS_2 [35].

In summary, the ground state of Cu_2Se, typified by Se-Cu-Cu-Cu-Cu-Se sextuple layers, has been identified using *ab initio* calculations. Upon cooldown to liquid nitrogen temperatures, the transport property measurements along with the structural analyses have confirmed the existence of yet another phase transition of possible CDW character. The unusual manifestation of the WAL-type of MR profile at liquid helium temperatures indicates the quantum nature of such a phase of Cu_2Se, which may promote further interest in this member of the TMCs.

[1] Q. H. Wang, K. Kalantar-Zadeh, A. Kis, J. N. Coleman, and M. S. Strano, Nat. Nano **7**, 699 (2012).

[2] R. Xu, A. Husmann, T. F. Rosenbaum, M. L. Saboungi, J. E. Enderby, and P. B. Littlewood, Nature **390**, 57 (1997).

[3] W. Zhang, R. Yu, W. X. Feng, Y. G. Yao, H. M. Weng, X. Dai, and Z. Fang, Phys. Rev. Lett. **106**, 156808 (2011).

[4] B. Sipos, A. F. Kusmartseva, A. Akrap, H. Berger, L. Forro, and E. Tutis, Nat. Mater. **7**, 960 (2008).

[5] H.-Z. Lu, W. Yao, D. Xiao, and S.-Q. Shen, Phys. Rev. Lett. **110**, 016806 (2013).

[6] H. Yuan, M. S. Bahramy, K. Morimoto, S. Wu, K. Nomura, B.-J. Yang, H. Shimotani, R. Suzuki, M. Toh, C. Kloc, X. Xu, R. Arita, N. Nagaosa, and Y. Iwasa, Nat. Phys. **9**, 563 (2013).

[7] H. Liu, X. Shi, F. Xu, L. Zhang, W. Zhang, L. Chen, Q. Li, C. Uher, T. Day, and G. J. Snyder, Nat. Mater. **11**, 422 (2012).

[8] S. C. Riha, D. C. Johnson, and A. L. Prieto, J. Am. Chem. Soc. **133**, 1383 (2010).

[9] X. Xiao, W. Xie, X. Tang, and Q. Zhang, Chin. Phys. B **20**, 087201 (2011).

[10] H. Liu, X. Yuan, P. Lu, X. Shi, F. Xu, Y. He, Y. Tang, S. Bai, W. Zhang, L. Chen, Y. Lin, L. Shi, H. Lin, X. Gao, X. Zhang, H. Chi, and C. Uher, Adv. Mater. **25**, 6607 (2013).

[11] Landolt-Börnstein, in *Non-Tetrahedrally Bonded Elements and Binary Compounds I*, Vol. 41C (Springer, Berlin, Heidelberg, 1998), p. 1.

[12] T. Ohtani, Y. Tachibana, J. Ogura, T. Miyake, Y. Okada, and Y. Yokota, J. Alloys Compd. **279**, 136 (1998).

[13] H. Chi, H. Kim, J. C. Thomas, X. Su, S. Stackhouse, M. Kaviany, A. Van der Ven, X. Tang, and C. Uher, Phys. Rev. B **86**, 195209 (2012).

[14] G. Kresse and J. Furthmüller, Phys. Rev. B **54**, 11169 (1996).

[15] J. P. Perdew, K. Burke, and M. Ernzerhof, Phys. Rev. Lett. **77**, 3865 (1996).

[16] P. E. Blöchl, Phys. Rev. B **50**, 17953 (1994).

[17] G. Kresse and D. Joubert, Phys. Rev. B **59**, 1758 (1999).

[18] J. Heyd, G. E. Scuseria, and M. Ernzerhof, J. Chem. Phys. **118**, 8207 (2003).

[19] A. V. Krukau, O. A. Vydrov, A. F. Izmaylov, and G. E. Scuseria, J. Chem. Phys. **125**, 224106 (2006).

[20] K. Parlinski, PHONON software package (Cracow, 2008).

[21] G. K. Padam, Thin Solid Films **150**, L89 (1987).

[22] V. P. Kubaschewski and J. Nölting, Berich. Bunsen. Gesell. **77**, 70 (1973).

[23] M. C. Nguyen, J.-H. Choi, X. Zhao, C.-Z. Wang, Z. Zhang, and K.-M. Ho, Phys. Rev. Lett. **111**, 165502 (2013).

[24] M. Råsander, L. Bergqvist, and A. Delin, J. Phys.: Condens. Matter **25**, 125503 (2013).

[25] N. Frangis, C. Manolikas, and S. Amelinckx, Phys. Status Solidi A **126**, 9 (1991).

[26] A. L. N. Stevels and F. Jellinek, Recueil **90**, 273 (1971).

[27] M. A. Korzhuev, V. F. Bankina, B. F. Gruzinov, and G. S. Bushmarina, Sov. Phys. Semicond. **23**, 959 (1989).

[28] S. A. Danilkin, M. Avdeev, T. Sakuma, R. Macquart, and C. D. Ling, J. Alloys Compd. **509**, 5460 (2011).

[29] J. S. Rhyee, K. H. Lee, S. M. Lee, E. Cho, S. Il Kim, E. Lee, Y. S. Kwon, J. H. Shim, and G. Kotliar, Nature **459**, 965 (2009).

[30] S. Hikami, A. I. Larkin, and Y. Nagaoka, Prog. Theor. Phys. **63**, 707 (1980).

[31] B. A. Assaf, T. Cardinal, P. Wei, F. Katmis, J. S. Moodera, and D. Heiman, Appl. Phys. Lett. **102**, 012102 (2013).

[32] J. Chen, H. J. Qin, F. Yang, J. Liu, T. Guan, F. M. Qu, G. H. Zhang, J. R. Shi, X. C. Xie, C. L. Yang, K. H. Wu, Y. Q. Li, and L. Lu, Phys. Rev. Lett. **105**, 176602 (2010).

[33] M. Liu, J. Zhang, C.-Z. Chang, Z. Zhang, X. Feng, K. Li, K. He, L.-l. Wang, X. Chen, X. Dai, Z. Fang, Q.-K. Xue, X. Ma, and Y. Wang, Phys. Rev. Lett. **108**, 036805 (2012).

[34] L. Bao, L. He, N. Meyer, X. Kou, P. Zhang, Z. Chen, A. V. Fedorov, J. Zou, T. M. Riedemann, T. A. Lograsso, K. L. Wang, G. Tuttle, and F. Xiu, Sci. Rep. **2**, 726 (2012).

[35] S. Tongay, H. Sahin, C. Ko, A. Luce, W. Fan, K. Liu, J. Zhou, Y.-S. Huang, C.-H. Ho, J. Yan, D. F. Ogletree, S. Aloni, J. Ji, S. Li, J. Li, F. M. Peeters, and J. Wu, Nat. Commun. **5**, 3252 (2014).